



Chitosan–Gelatin @ Tin (IV) Tungstatophosphate Nanocomposite Ion Exchanger: Synthesis, Characterization and Applications in Environmental Remediation

Kuljit Kaur¹ · Rajeev Jindal¹ · Riteeka Tanwar¹

Published online: 16 October 2018

© Springer Science+Business Media, LLC, part of Springer Nature 2018

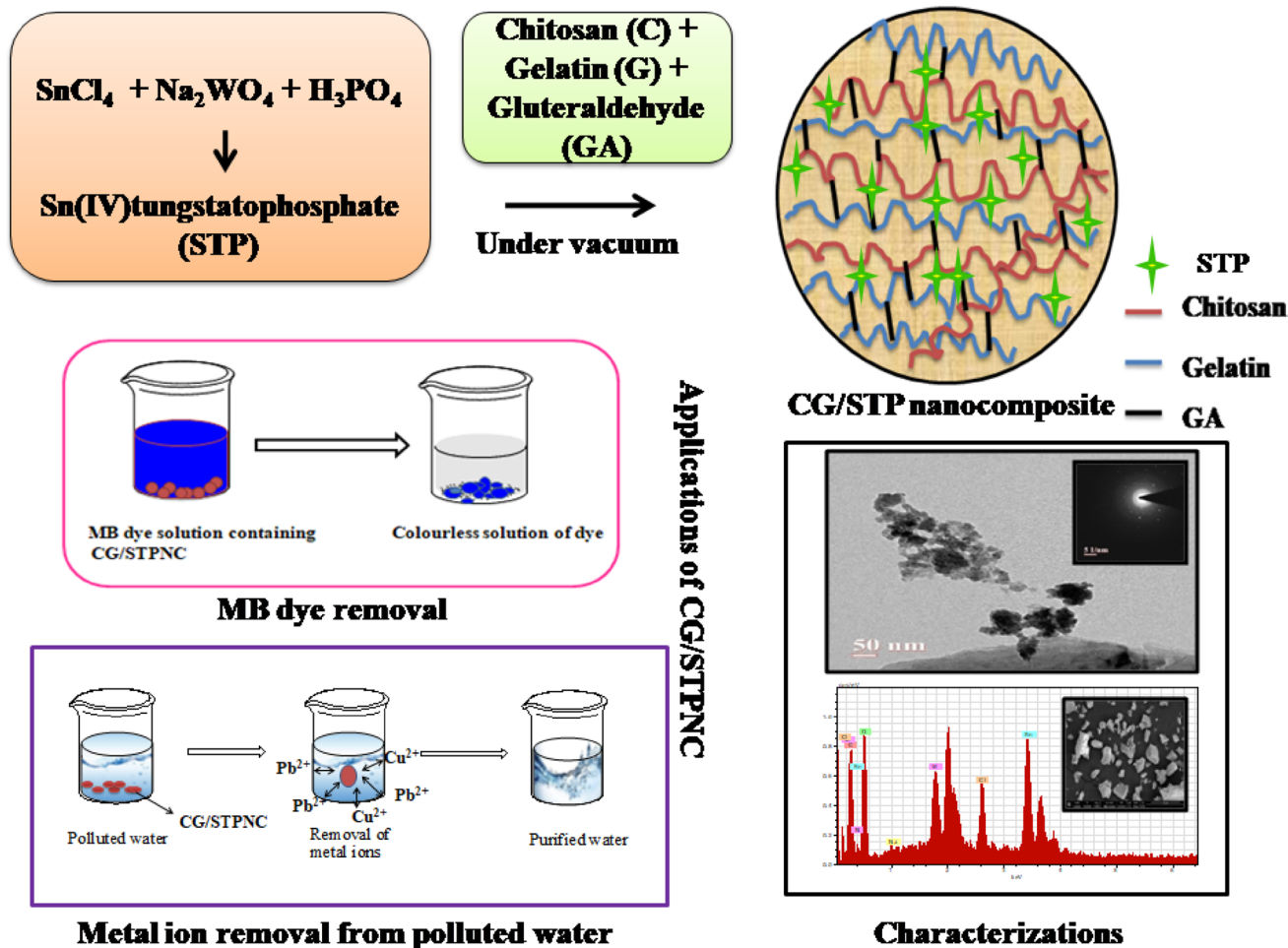
Abstract

The present study reported the synthesis of novel organic–inorganic hybrid nanocomposite by incorporating tin (IV) based ion exchanger into the hybrid polymer network of chitosan and gelatin prepared under vacuum for the efficient removal of heavy metal ions and toxic dyes from an aqueous fluid. The physicochemical studies such as ion exchange capacity (IEC), chemical stability, thermal stability, pH titration and distribution behaviour studies were also carried out to determine the cation exchange behaviour of the material. The surface morphology and structural properties were studied by the techniques such as FTIR, FESEM, EDS, TEM and XRD. Distribution studies confirmed the synthesized CG/STPNC had the highest selectivity for Pb^{2+} ions (85.3 mL/g). Maximum adsorption of methylene blue (82%) was achieved within 240 min at 500 mg of adsorbent dose, 10 mg/L of the initial concentration of dye, pH of 7 and 30 °C of temperature. Adsorption kinetic data fitted well with pseudo-second order rate model with $R^2 = 0.995$. The correlation value 0.95 and favourable $R_L = 0.21$ of adsorption data suggested better fit for Langmuir adsorption. Thus the synthesized nanocomposite ion exchanger was found to be a promising cation exchanger as well as an adsorbent for heavy metal ion and dye removal from textile industrial effluents.

✉ Rajeev Jindal
jindalr@nitj.ac.in

¹ Department of Chemistry, Dr B R Ambedkar National Institute of Technology, Jalandhar, Punjab 144011, India

Graphical abstract



Keywords Nanocomposite · Ion exchanger · Heavy metals · Methylene blue and ion exchange capacity

Abbreviations

C	Chitosan
G	Gelatin
HPN	Hybrid polymer network
GLA	Glutaraldehyde
IEC	Ion exchange capacity
CG/STPNC	Chitosan–gelatin/Sn(IV)tungstatophosphate nanocomposite
STP	Sn (IV) tungstatophosphate
MB	Methylene blue

Introduction

Over two-thirds of the earth surface is covered with water and undeniably, it has become one of the greatest resources. Presently, the increase in population and industrial waste ultimately causes water pollution. Various organic and inorganic pollutants are responsible for causing water pollution due to their toxic and carcinogenic nature [1]. Over the past few years, the rampant use of dyes in industries is the major cause of water pollution because of the release of the dyes in the water [2, 3]. Dyes have complex stable aromatic structures and are synthetically prepared. They have poor degradability in the environment causing various ecological problems. These highly toxic dyes used in a large number of industries such as textiles, paper, plastics and cosmetics [4, 5]. A large number of processes have emerged for

the removal of dyes like biological treatment, coagulation, floatation, electrochemical techniques, adsorption and oxidation [6–12]. Among all, adsorption route is the most widely used method because of the easy availability of different adsorbents [13]. Thus, dye removal has been emerged as a dire need for wastewater treatment and reducing the aquatic concern of toxicity [14]. A large number of heavy metals like lead, antimony, mercury, cadmium, cobalt, nickel etc. are discharged into the water from mining, pharmaceuticals, bleaching and tannery, and metal finishing industries [15–19]. These heavy metals are hazardous to human beings as they can enter the food chain causing poisonous effects [20, 21]. As a consequence, it has become essential to eradicate heavy metal ions and dyes before being released into the water. Of late, ion-exchangers have been widely used in the field of dye removal because of their good ion exchange capacity, cost effectiveness and high distribution coefficient values. Ion exchangers are the insoluble solid substance, which has the tendency to exchange ions from the electrolyte and release ions of the same charge into the solution [22]. Different kind of inorganic and organic ion exchangers has already been explored by number of researchers to remove the poisonous pollutants [23–25]. Organic ion exchanger consists of a three-dimensional cross-linked matrix containing acidic or basic groups. These resins have both cation and anion exchange property. Cation exchange resins consist of strongly acidic $-\text{SO}_3\text{H}$ group, moderately acidic $-\text{CO}_2\text{H}$ or the weakly acidic $-\text{OH}$ group. Anion-exchange resins contain weak amino groups. In inorganic ion exchangers, the matrix consists of the inorganic part, which can act as oxidative and reducing agents. Organic ion exchangers are the widely known because of its good ion exchange capacity and stability [26]. However, inorganic ion exchangers are stable even at a high temperature than organic ion exchangers and therefore are applicable in metal ion absorption and catalysis [27]. However, there are certain limitations existing with them, which prevent their use in the removal of heavy metals. To overcome the limitations, hybrid ion-exchangers have been synthesized by incorporating inorganic precipitates within the organic matrix [28]. These organo-inorganic composites are of great interest because of their high mechanical strength, stability and high performance. They show high ion exchange capacity and are used in heavy metal ion removal applications.

Recently, nanocomposite ion exchangers have trapped enormous interest of the scientific community due to the widespread utility in various fields such as water softening, dye removal, chromatography, separation of heavy metal ions from effluents and ion selective electrodes etc due to their marvelous properties as compare to the bulk materials like excellent adsorbents because of advantages of possessing higher adsorption capacity [5, 29–35]. Gelatin (G) is one of the most important natural biological macromolecule material derived

from the hydrolysis of collagen; it has been widely used in food, medicine and chemical industry [36]. However, lack of mechanical properties restricts the use of gelatin as natural biomaterials. Chemical cross-linking of gelatin with natural polymers like chitosan (C) may provide a simple method to improve the chemical stability and mechanical strength [37]. Chitosan (C) has been used by a number of researchers worldwide for removal of various pollutants from the environment. Hydrogels, nanogels and nanocomposite materials of chitosan and modified chitosan have been found extensive applications in the field of adsorption of dyes, removal of metal ions, and photodegradation of organic pollutants in wastewater [38–40]. As per the literature survey and the best of our knowledge, there is no report on the under vacuum synthesis of the chitosan and gelatin-based HPN. The novelty of work lies in the under vacuum synthesis of nanocomposite ion exchanger of chitosan and gelatin with the incorporation of tin (IV) tungstatophosphate inorganic ion exchanger. In the present study, an attempt has been made to explore the use of biopolymers like chitosan and gelatin in the synthesis, characterization and application of nanocomposite ion exchanger based upon Sn(IV) tungstatophosphate (under vacuum). Under vacuum, condition was chosen for the synthesis of nanocomposite ion exchanger because mostly the free radical polymerization reactions required for hydrogel formation are inhibited to a large extent by the presence of oxygen in air condition. Therefore, for preparing the nanocomposite ion exchanger, the vacuum condition is appropriate because it provides the environment with minimum oxygen content [41, 42]. The synthesized CG/STPNC ion exchanger was effectively characterized by different characterization techniques like FTIR, XRD, FE-SEM and HRTEM. CG/STPNC was explored for the selective removal of Pb^{2+} and Cu^{2+} metal ions. The nanocomposite ion exchanger was further used to remove methylene blue dye from wastewater. Methylene blue considered as the most widely used dye for dyeing cotton, wood and silk [43]. MB is the toxic cationic dye having positive nitrogen atom and show an adverse effect on human health such as vomiting, diarrhoea, heart rate, cyanosis, jaundice, gastritis and breathing problem [44]. Thus, it has become the essential need to remove methylene blue before it is discharged in the water and cause pollution. Therefore, the present research work is of immense scientific and industrial interest to remove lethal dyes and heavy metals from contaminated water resources.

Materials and Methods

Materials

Chitosan, gelatin, acetic acid, stannic chloride (SnCl_4), sodium tungstate (Na_2WO_4), orthophosphoric acid (H_3PO_4), nitric acid (HNO_3), sodium hydroxide (NaOH), EDTA,

Eriochrome black-T, methyl orange, methylene blue were purchased from HiMedia, India. Glutaraldehyde was purchased from Merck Specialties Private Limited (Mumbai, India). Metal nitrates such as cupric nitrate, lead nitrate, nickel nitrate and magnesium nitrate have been purchased from SD Fine Pvt. Ltd, India. All reagents are of analytical grade and used without any further refinement.

Instrumentation

Fourier transform infrared (FTIR) spectrophotometer a (Perkin Elmer spectrophotometer), Field Emission Gun SEM (Nova Nano FE-SEM 450 FEI), UV–VIS spectrophotometer (Systronics Double Beam UV–VIS Spectrophotometer 2201), XRD panalytical X'Pert Pro multipurpose diffraction (MPD), Transmission Electron Microscope (The Tecnai G² 20 (FEI) S-Twin), Brunauer-Emmett-Teller (BET) analysis used for calculation of surface area (N₂ physisorption) were used for the characterization of the synthesized samples.

Preparation of solvents

0.1 M nitric acid, 0.1 M stannic chloride, 0.1 M sodium tungstate and 0.1 M orthophosphoric acid were prepared by adding the calculated amount in the required amount of distilled water.

Preparation of organo-inorganic hybrid nanocomposite (CG/STPNC) ion exchanger

Inorganic precipitates of Sn (IV) tungstatophosphate were synthesized by adding 0.1 M stannic chloride, 0.1 M orthophosphoric acid and 0.1 M sodium tungstate in different volume ratios as shown in Table 1. The precipitates of prepared hybrid ion exchanger were then filtered off, washed with distilled water and dried. These precipitates were then incorporated into the polymeric network of chitosan and gelatin. The reaction was carried out in the vacuum oven with the addition of the calculated amount of crosslinker at pre-optimized conditions of temperature, pressure and time. The synthesized product was then dried in a hot air oven at 50 °C. The dried product was then crushed into small granules and dipped in 0.1 M nitric

acid (HNO₃) for 24 h. The prepared ion exchangers then washed with distilled water to remove excess of acid and then dried again at 50 °C in the oven.

Instrumental Analysis

Fourier Transform Infrared (FTIR)

FTIR spectrum of the samples was recorded in the range of 400–4000 cm⁻¹ using KBr disc method in Perkin Elmer spectrophotometer. A disc of the nanocomposite in the H⁺ form was formed by applying a pressure of 6894.76 Pa in moisture free atmosphere. This technique provides the information about sample structure and functional groups.

Field Emission Scanning Electron Microscopy–Energy Dispersive Spectroscopy (FESEM–EDS)

The surface morphology of the synthesized hydrogel, inorganic ion exchanger and CG/STPNC ion exchanger, were viewed in Nova Nano FE-SEM 450. Samples of nanocomposite were gold-plated to achieve good conductive effects. EDS was used to measure the elemental composition of the sample of hydrogel and nanocomposite ion exchanger.

High-Resolution Transmission Electron Microscope (HR-TEM)

The high-resolution images of the prepared hybrid nanocomposite were recorded in Tecnai G² 20 (FEI) transmission electron microscope. It was used for identification of size and particles. The sample for TEM was prepared by dispersing nanoparticles for 1–2 h in ultrasonicator and placed over Cu grid for determination of particle size and morphology. Selected area electron diffraction (SAED) images in TEM studies are very important tools to determine the crystal structure of any material in which the electrons are diffracted at a particular selected area and bright spots with a dark background are observed.

Table 1 Variation of volumes of different inorganic ions

Sample	Molar concentration (mol/L)			Volume ratios	pH	I.E.C (meq/g)
	Sn ⁴⁺	WO ₄ ²⁻	PO ₄ ³⁻			
STP1	0.1	0.1	0.1	2:1:1	7	1.8
STP2	0.1	0.1	0.1	1:1:1	7	0.2
STP3	0.1	0.1	0.1	1:1:2	7	0.8
STP4	0.1	0.1	0.1	1:2:1	7	0.6
STP5	0.1	0.1	0.1	3:1:1	7	1.6

X-Ray Diffraction (XRD)

X-ray diffraction studies of nanocomposite, ion exchanger and hydrogel were carried out in powdered XRD by using panalytical X'pert multipurpose diffraction (MPD) with Cu-K α radiation of wavelength 1.54 Å at 298 K. XRD studies use to depict the crystallinity and amorphous nature of the sample (Bale et al. 1998).

Physicochemical properties

Ion exchange capacity

Ion exchange capacity of the hybrid ion exchanger (CG/STPNC) was determined by the standard column chromatography as discussed in the literature [20]. 1 g of CS/STPNC in H⁺ was placed in glass column supported with glass wool at the bottom of the column. A 1M solution of KCl was added as an eluent and allowed to pass through the ion exchangers at the rate of 10 drops per minute. The added eluent was passed through the exchanger until all the H⁺ ions were replaced and were confirmed by checking pH of the effluent. The process was repeated with other alkali or alkaline metal solutions as an eluent. The collected effluent with replaced H⁺ ions was then titrated with 0.1 M NaOH and phenolphthalein used as an indicator. The ion exchange capacity was calculated by using the following formula as in Eq. 1:

$$\text{I.E.C} = \frac{N \times V}{W} \text{ mequiv/g} \quad (1)$$

where N is the normality, V is the volume of alkali used and W is the weight of nanocomposite ion exchanger occupied.

pH Titrations Studies

pH titration study of CG/STPNC ion exchanger was performed by the method mentioned in literature [29]. 0.5 g of the ion exchanger in its H⁺ form was equilibrated with 50 mL of the equimolar solutions of metal chlorides and their hydroxides (KCl with KOH and NaCl with NaOH) were placed in a conical flask in different volume ratios. The pH was recorded after 24 h until equilibrium was achieved.

Thermal Stability

Thermal stability of ion exchangers was determined at different temperatures. In this method, 0.5 g of ion exchanger (H⁺ form) was heated at different temperature ranges from 100 °C to 500 °C for 1 h in a muffle furnace. After cooling down at room temperature, ion exchange capacity was calculated by the method discussed in Sect. 2.6.1.

Chemical Stability

Chemical stability of ion exchangers for different chemical solutions was studied. In this method, 500 mg of ion exchanger was equilibrated with different chemical solutions for 24 h at room temperature. After this, the solution was washed and filtered off to remove excess acid or base. The remaining ion exchangers have then washed again with distilled water and dried in a hot oven at 40 ± 10 °C till constant weight. The ion exchange capacity was then again calculated by column method.

Distribution Studies

The distribution study of the metal ions plays a crucial role in the selectivity of the prepared ion exchanger. The batch method was used to determine the distribution coefficient (K_d value) of the ion exchanger in different solvent solutions. 0.2 g of CG/STPNC ion exchanger in its H⁺ form was added in 20 mL of metal nitrate solutions with discontinuous shaking 24 h in a shaker. The concentration of metal ions was determined before and after the equilibrium by titrating with EDTA solution. K_d values of metal ions were calculated by using the formula mention below in Eq. (3) [21]

$$K_d = \frac{I - F}{F} \times \frac{V}{M} \text{ mL/g} \quad (2)$$

where I is the initial amount and F is the final amount of metal ions in an aqueous phase, V is the volume of the solution and m is the mass of the ion exchanger (g).

Applications of CG/STPNC Ion Exchanger in Dye Removal Studies

The adsorption studies of methylene blue (MB) dye removal were performed by the batch method. Solutions of different concentrations ranging from 2 to 10 mg/L were prepared. The hybrid nanocomposite was added to the 100 mL solution of the dye. The effects of adsorption were studied by varying dye concentrations, pH, sample concentration and temperature. The amount of dye adsorbed per unit mass of sample (q_t) was calculated by using the formula in Eq. (3)

$$q_t = \frac{(C_o - C_t)V}{M} \quad (3)$$

where V is the volume of the dye solution, M is the mass of the dry sample, C_o is the initial concentration of MB and C_t is the concentration of MB at time t.

The percentage dye removal was calculated using the Eq. (4)

$$\%R = \frac{(C_o - C_e)}{C_o} \times 100 \quad (4)$$

where C_e is the concentration of MB at equilibrium.

Results and Discussions

Mechanism

The mechanism of the formation of the HPN matrix occurs through the formation of the Schiff's base. A Schiff base is a nitrogen analogue of an aldehyde or ketone in which the C=O group is replaced by C=N–R group. It is usually formed by condensation of an aldehyde or ketone with a primary amine. Here Schiff base is formed by reaction among chitosan and gelatin polymeric chains in the presence of an acid as catalyst and glutaraldehyde as cross-linker [45]. The network formed by the cross linking of two same polymeric chains or different polymeric chains with glutaraldehyde. Figure 1a shows the mechanism of formation of HPN matrix where both chitosan and gelatin are linked with each other by the crosslinking through glutaraldehyde to form a 3D network. Figure 1b shows the structure of the prepared inorganic ion exchanger. The prepared inorganic ion exchanger was incorporated into the chitosan and gelatin mixture during the synthesis of HPN. Inorganic ion exchanger has shown various physical interactions with the polymeric chains containing functional groups in 3D HPN matrix and results in the formation of nanocomposite (Fig. 1c).

Physico-Chemical Properties

Ion exchange capacity used to determine the number of H^+ ions replaced by the CG/STPNC. It is determined by the column method as mentioned earlier in Sect. 2.6.1. Ion exchange capacity of various samples prepared by varying different volume ratios was determined. Table 1 show that the SWP 1 ion exchanger has the better exchange capacity (1.8 mequiv/g) among all. Its IEC was found to be much higher than its inorganic counterpart (1.0 mequiv/g). Therefore, this sample of ion exchanger was further used for the study of various other physicochemical properties. It can be explained on the basis of binding of an organic part with the STPNC which results in the increased surface area and enhanced ion exchange capacity. The pH titration curve (Fig. 2) of the CG/STPNC ion exchanger shows that H^+ ions were replaced into the basic equimolar solutions of alkali metal chlorides and their hydroxides (KCl with KOH and NaCl with NaOH) [46, 47]. As the volume of the base (KOH and NaOH) increased in the solution, OH^- ions concentration was also increases and this increased concentration was replaced by the released H^+ ions. As the basicity of the medium increases, the rate of ion exchange also increases due to the removal of all H^+ ions from the solution.

The curve (Fig. 2) shows one inflexion point indicating the bifunctional behaviour of the ion exchanger.

Thermal stability of the synthesized nanocomposite ion exchanger was determined by calculating ion exchange capacity of the hybrid ion exchanger heated at a different temperature. It can be investigated from the Table 2 that the ion exchange capacity of the prepared ion exchanger decreases with increase in temperature due to the degradation of the organic counterpart and physical denaturation of the nanocomposite ion exchanger at molecular and macroscopic level. The CG/STPNC was found to possess average thermal stability as it possessed about 33.3% (0.4 mequiv/g, Table 2) of the initial IEC (1.4 mequiv/g, Table 1) by heating up to 400 °C.

The effect of various chemicals at different concentrations on ion exchange capacity was shown in Table 3. These studies of the chemical stability of CG/STPNC revealed that the weight of nanocomposite ion exchangers gets lowered on treatment with different acidic and basic solutions for 24 h. The prepared nanocomposite ion exchanger was quite stable in mineral acids at low concentration (1M HCl, 1M HNO_3) but begin to dissociate at higher concentrations of acids and at all concentration of bases. At a very high concentration of base, a complete dissolution of the crosslinked network of CG/STPNC ion exchanger takes place.

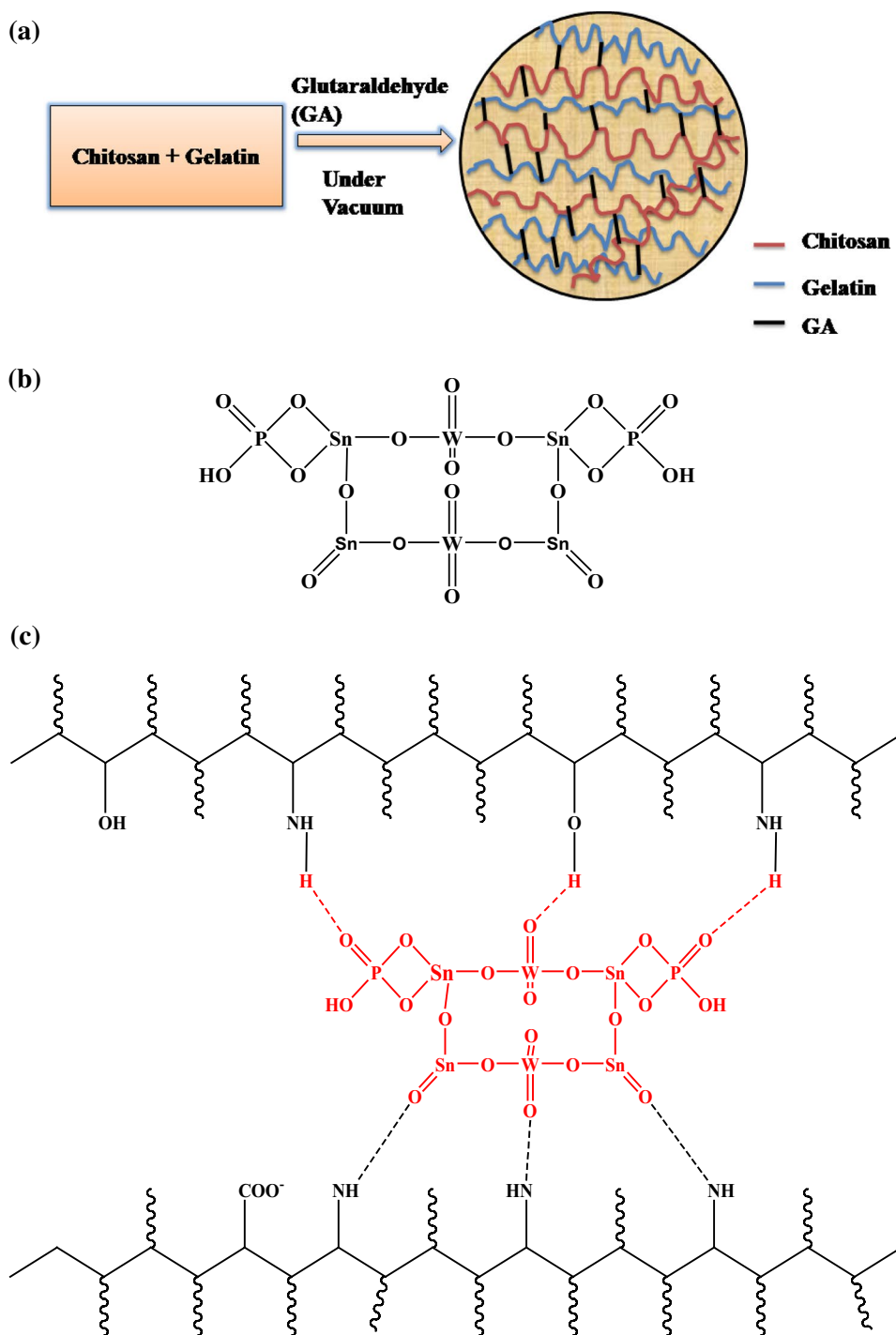
Table 4 shows the distribution coefficients values of different heavy metal ion solutions. The distribution studies explained the cation exchange potential of different metal nitrates in the separation of the metal ions from the solution. The distribution coefficient (K_d) values were strength and solvent dependent [48]. The selectivity of metal ions was obtained in distilled water and the order was $Pb^{+2} > Cu^{+2} > Ni^{+2} > Mg^{+2}$.

Ion exchange capacity was found the maximum for the potassium ion (Table 5). It has 1.4 meq/g of ion exchange capacity due to its appropriate size with the exchanger it was easily replaced for the solution of potassium chloride. Thus, potassium ion showed the high tendency to exchange ion with the ion exchanger used.

Characterizations

The surface morphology of CG hydrogel of chitosan and gelatin and hybrid nanocomposite was studied (Fig. 3a, b). Both the samples showed the remarkable difference in their morphology. The surface of the CG hydrogel found to be less porous and rough than the CG/STPNC. Synthesized nanocomposite ion exchanger was found to be highly porous, rough and heterogeneous because of incorporation of ion exchanger along with the cross-linking in the backbone chains. The FE-SEM of CG/STPNC before and after adsorption of MB was compared (Fig. 3b, c) and it was observed that after adsorption, the morphology of the CG/STPNC ion

Fig. 1 a Mechanism of the formation of cross linked network of Chitosan and gelatin. **b** Structure of Sn (IV) tungstatophosphate ion exchanger. **c** Mechanism for the synthesis of CG/STPNC nanocomposite ion exchanger



exchanger gets modified. The MB dye gets adsorbed on the surface of the adsorbent and made it less porous than before.

Energy dispersive X-ray spectroscopic studies (Fig. 3d, e) of CG hydrogel confirms the C, N and O but EDS spectra of CG/STPNC showed various elemental peaks of C, N, O, W, Sn, P and Na present in it which confirmed the incorporation of inorganic ion exchanger into the organic counterpart and results in the formation of hybrid ion exchanger.

High-resolution transmission electron microscopic images of CG/STPNC ion exchanger are shown in Fig. 3f to g. The dark region in the TEM image showed chitosan and gelatin wrapped in the STP ion exchanger, whereas the light portion indicated chitosan and gelatin. The TEM images of nanocomposite confirm the particle size in the range of 20–90 nm with ImageJ software. Selected Area Electron Diffraction (SAED) image of CG/STPNC ion exchanger has

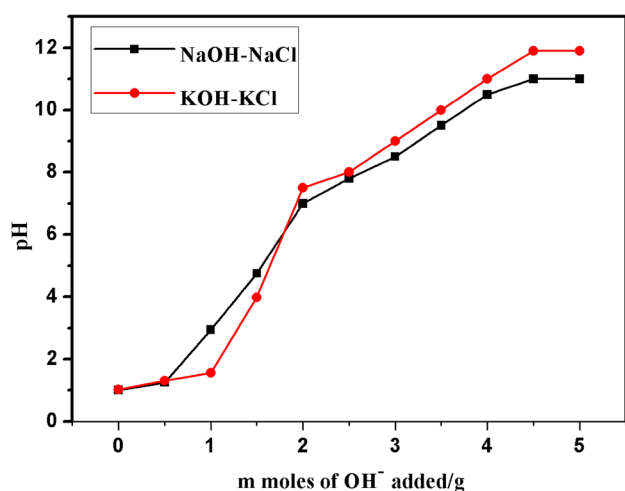


Fig. 2 pH titrations curves of NaOH and KOH

Table 2 Effect of temperature on I.E.C of CG/STPNC

S. no	Temperature (°C)	Colour	I.E.C (meq/g)
1	100	Brown	1.2
2	200	Brown	0.9
3	300	Brown	0.6
4	400	Black	0.4
5	500	Black	0.2

Table 3 Chemical stability of CG/STPNC in different solvents and its effect on ion exchange capacity

S.no.	Solution	Initial weight (g)	Final weight (g)	I.E.C (meq/g)
1	0.1 M HCl	0.5	0.387	1.6
2	1M HCl	0.5	0.382	1.0
3	2M HCl	0.5	0.345	0.8
4	0.1M HNO ₃	0.5	0.412	1.8
5	1M HNO ₃	0.5	0.396	1.6
6	2M HNO ₃	0.5	0.367	1.2
7	1M NaOH	0.5	0.132	0.5
8	2M NaOH	0.5	Dissociates completely	-
9	1M KOH	0.5	0.152	0.6
10	2M KOH	0.5	Dissociates completely	-

been shown in Fig. 3h. It is clear from SAED pattern that the sample seems to be nanocrystalline (with very small crystallite sizes) with the bright lattice spots in high-resolution TEM which confirmed that CG/STPNC ion exchanger contained short range crystallinity [49].

Table 4 K_d value of different metal ions in metal nitrates on CG/STPNC in different solvents

S. no.	Metal ions	K_d value (mL/g)	
		D.W	0.1 M HCl
1	Pb ²⁺	85.3	78.2
2	Cu ²⁺	65.2	58.8
3	Mg ²⁺	13.33	12.1
4	Ni ²⁺	20.4	16.4
5	Ca ²⁺	35.8	24.7

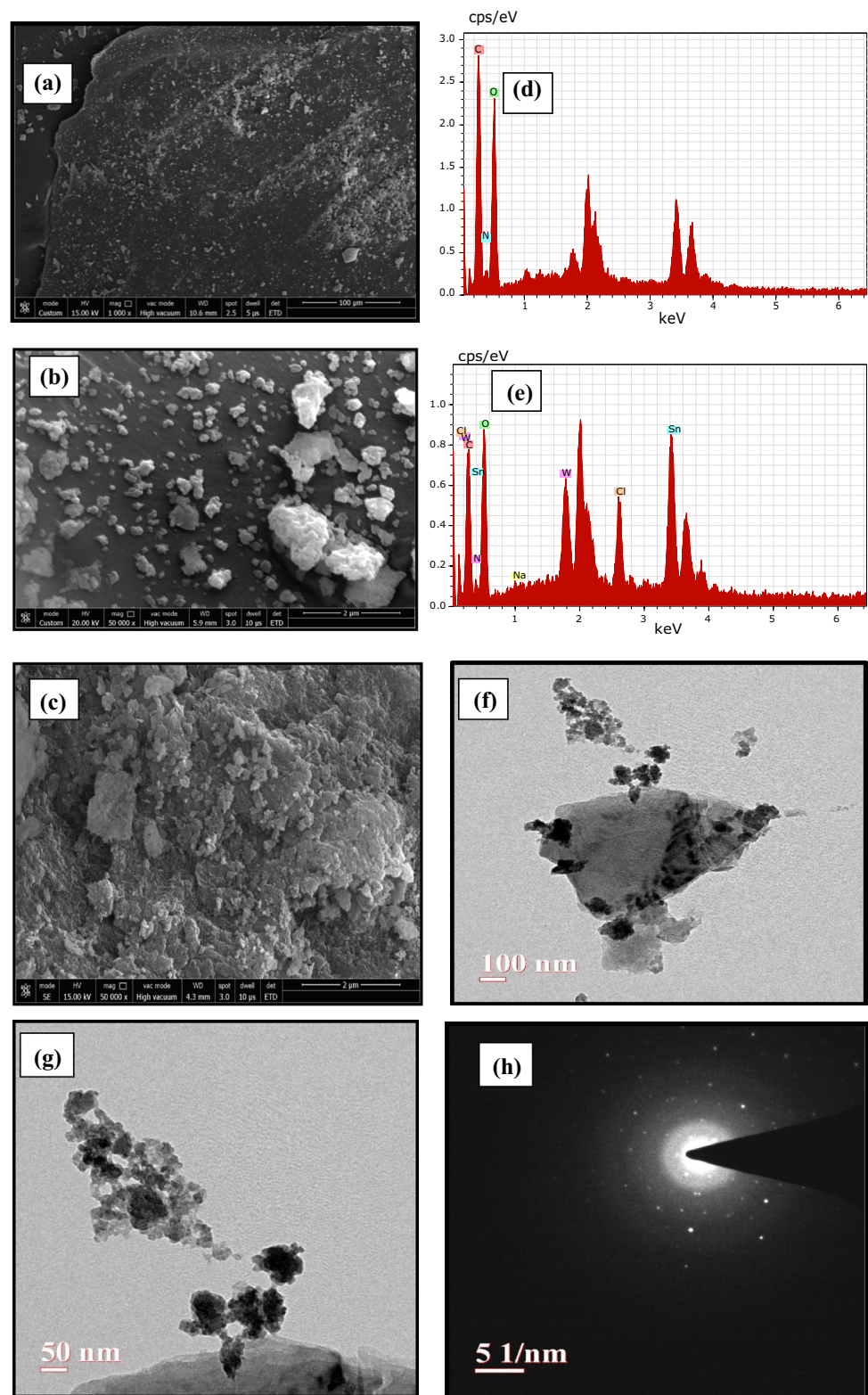
Table 5 Ion-exchange capacity of various exchanging ions

S. no.	Exchanging ions	I.E.C (meq/g)
1	K ⁺	1.8
2	Na ⁺	1.6
3	Li ⁺	1.0
4	Mg ⁺²	0.8
5	Ca ⁺²	0.6

The FTIR spectrum (Fig. 4a) of the CG hydrogel matrix depicted a broad peak observed around 3500–3000 cm⁻¹ due to the overlapping of N–H and O–H stretching and 2883 cm⁻¹ due to C–H stretching vibrations. CG hydrogel matrix showed the significant peak at 1632 cm⁻¹ of C=N because of the formation of the imine bond. Thus, this peak confirms that the crosslinking in hydrogel takes place through Schiff's base formation. The IR spectrum of prepared ion exchanger (STP) recorded the peaks at 1026.6 cm⁻¹ of the ionic phosphate group and 509.7 cm⁻¹ of the Sn–O bond. However, the organo-inorganic nanocomposite CG/STPNC showed all characteristic peak at 3307 cm⁻¹, 1635 cm⁻¹, 1029.2 cm⁻¹ and 518.6 cm⁻¹ due to O–H and N–H stretch, C=N, PO₄³⁻ and Sn–O stretching vibrations respectively with the slight shift in wave numbers [50]. The small peak near 1250 cm⁻¹ may be attributed to C–N vibrations [51]. Thus the FTIR spectra of CG/STPNC confirmed the incorporation of inorganic counterpart into the CG hydrogel matrix and results in the formation of organic–inorganic hybrid nanocomposite ion exchanger.

The FTIR spectrum of CG/STPNC was compared before and after the adsorption of MB in the Fig. 4b. The FTIR spectrum of CG/STPNC after adsorption of MB depicted the peaks present in the spectrum of CG/STPNC after adsorption of MB are similar to the peaks present before adsorption but with change in the wave number along with the appearance of peaks of MB. The band appeared at 3100 cm⁻¹ confirmed the =C–H stretch of aromatic rings of MB in the FTIR spectra after adsorption [52]. The bands in the regions 1031 cm⁻¹ and 1250 cm⁻¹ were attributed to the bending vibrations of the C–N bond of aliphatic amines and to the

Fig. 3 FESEM images of **a** CG HPN matrix, **b** CG/STPNC before adsorption of MB, **c** CG/STPNC after adsorption of MB. EDS spectra of **d** CG HPN matrix, **e** CG/STPNC. TEM images of **e**, **f** CG/STPNC, SAED pattern of CG/STPNC



bending of the C–N bond of aromatic amines, respectively [53]. The bands in the region of 596 to 949.2 cm^{-1} were due to the deformation vibrations of C–H bond in polynuclear aromatic rings. The intensity of the broad peak in the

region of 3300 to 3600 cm^{-1} observed due to –OH and –NH₂ stretching vibration in the CG/STPNC before adsorption get lowered in the FTIR spectrum of CG/STPNC after adsorption which confirmed the interaction of these groups with

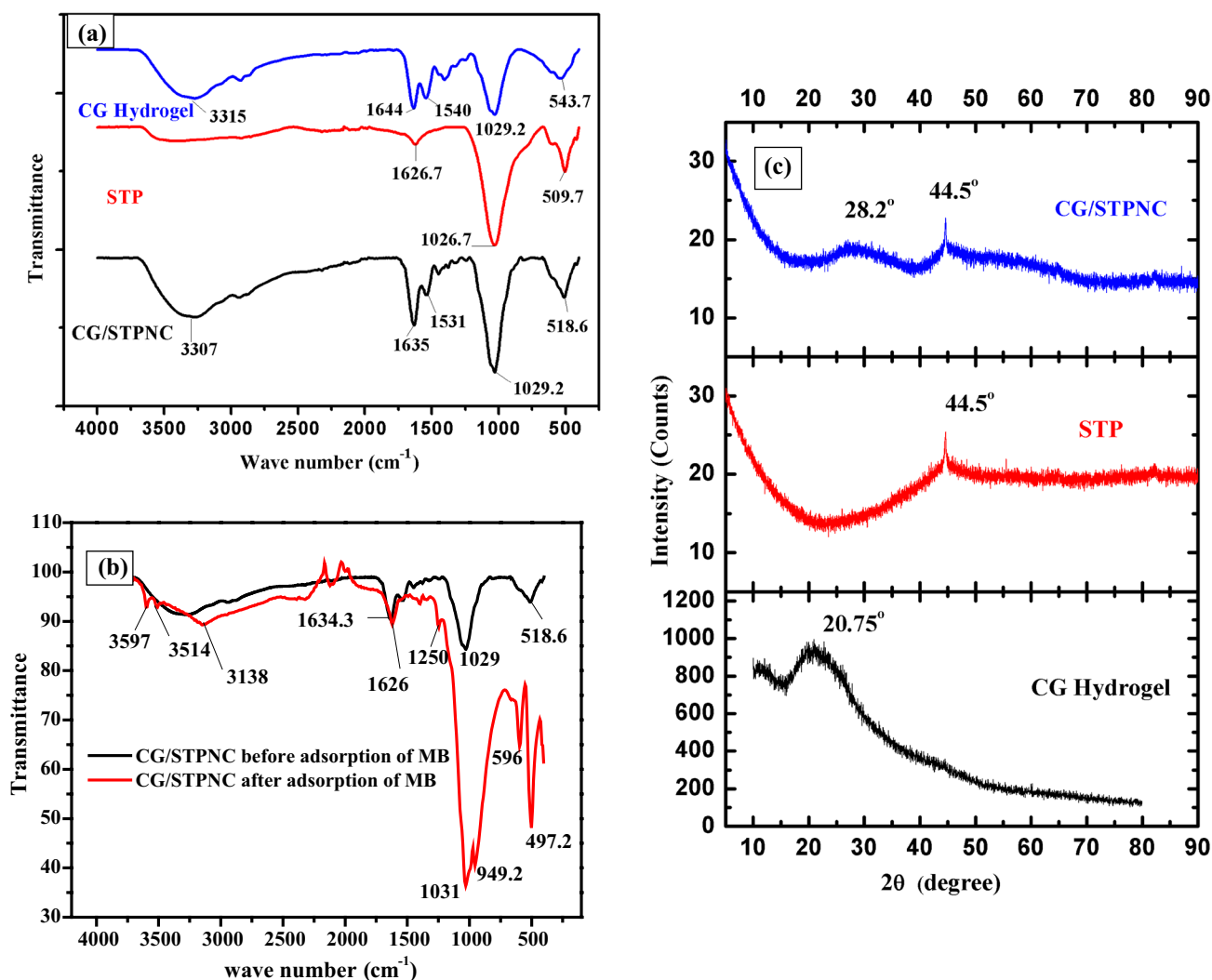


Fig. 4 **a** FTIR spectrum of CG HPN matrix, STP ion exchanger and CG/STPNC ion exchanger, **b** comparison of CG/STPNC ion exchanger before and after adsorption of MB. **c** XRD graphs of HPN matrix and CG/STPNC ion exchanger

MB dye. The other peaks of PO_4^{3-} , Sn–O and C=N groups get also shifted to 1031, 497.2 and 1626 cm^{-1} respectively confirmed the interaction between the surface of the adsorbent and dye molecules.

Powdered X-ray diffraction patterns of CG hydrogel, STP and CG/STPNC ion exchanger are shown in Fig. 4c. The powdered X-ray diffractogram of CG/STPNC exhibited all the peaks of CG hydrogel and STP ion exchanger with different intensities. The presence of a diffused peak of CG hydrogel and the peak of STP at 44.6° ion exchanger within the diffractogram of CG/STPNC confirmed the formation of nanocomposite ion exchanger. The low-intensity peaks assured the semi-crystalline nature of the CG/STPNC ion exchanger.

Surface area of the synthesized nanocomposite ion exchanger was estimated before and after adsorption of MB by using BET. The calculated surface area values for

both before and after adsorption of MB are 12.086 $\text{m}^2 \text{g}^{-1}$ and 12.340 $\text{m}^2 \text{g}^{-1}$ respectively. There was no much difference was observed in the surface area of both the samples might be due to the adsorption is monolayer and once the pores are covered (i.e. monolayer is formed) no more lateral interactions were observed for further adsorbate molecules and adsorbent was homogenous therefore the surface area remains almost same [54, 55]. Surface area was found > 10 m^2/g confirmed the meso porous nature of the adsorbent.

Application of CG/STPNC in dye removal (MB)

Mechanism

Methylene blue is the cationic dye and possesses quaternary amine group. This amine group has cationic nitrogen, which

interacts with the anionic part of the CG/STPNC adsorbent through electrostatic interaction (Fig. 5). In addition, adsorbent shows hydrogen bonding due to the presence of functional groups on it which strongly binds with the nitrogen of dye molecules. Thus, these interactions are responsible for the effective dye removal from aqueous solution.

Effects of Various Parameters on Dye Adsorption

Effect of Initial Concentration of Dye Initial concentration forms the important parameter for dye removal. The percentage removal of dye was found to increase with an increase in the initial concentration of it (Fig. 6a). This behaviour accounts for the prior attainment of the concentration gradient of the dye and ultimately results in the high removal of dye. The 10 mg/L concentration of dye showed the high percentage removal (82%) from aqueous solution.

Effect of Adsorbent Dose The percentage removal of dye also depends on the dose of the adsorbent. Higher is the adsorbent dose higher will be the removal of dye [56]. This behaviour is might be due to the increase in the surface area of the adsorbent, which results in more active sites on the adsorbent to adsorb the dye molecules. The percentage dye removal was studied by varying adsorbent dose from 200 to 700 mg. Figure 6b showed the maximum percentage removal for 600 mg of the adsorbent.

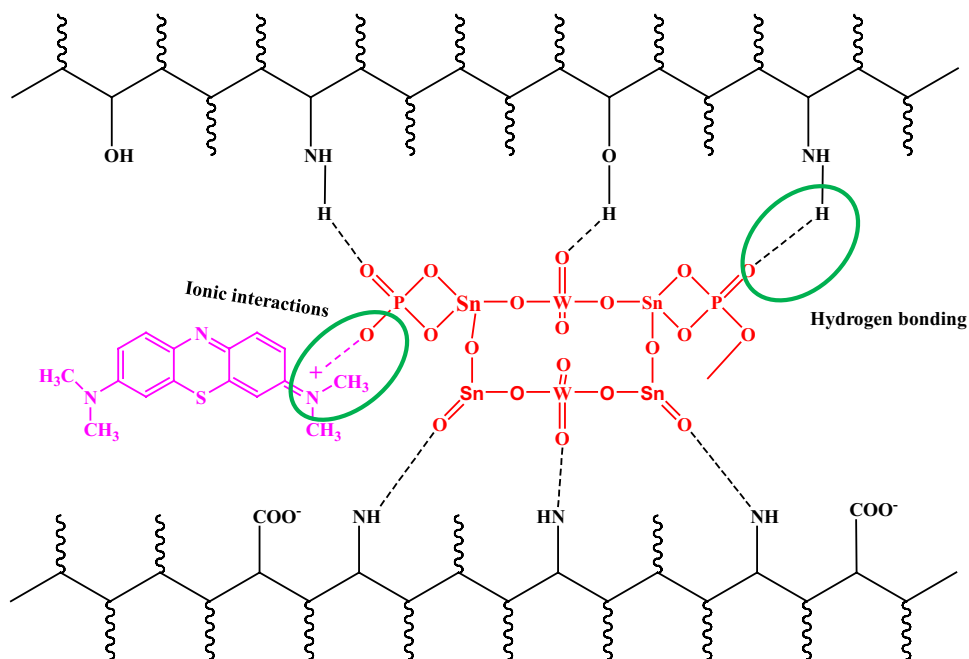
Effect of pH The effect of varying pH on the percentage dye removal was also studied in Fig. 6c and it plays the vital role in the determination of the adsorption capacity of adsor-

bent. pH was maintained from the acidic to the basic range (2–10). The percentage dye removal was maximum in the neutral range (pH = 7). At pH lower than 7 the protonation of amino groups ($-\text{NH}_2$) present in chitosan and gelatin results in increase in positive charge on adsorbent surface resulted in repulsions among polymeric chains and at pH more than 7 due to complete deprotonation of $-\text{NH}_3^+$ groups, the degree of ionization of the hydrogels is lowered, and there is a possibility of stronger and extensive hydrogen-bonding in the hydrogel matrix, as a result, the interaction with the dye molecule decreases and results in the decrease in the percentage dye removal [57]. This behaviour was expounded by the fact that at pH 7 the surface of the adsorbent contained favourable sites to interact with dye molecules and ultimately leads to the increase in percentage removal.

Effect of Temperature The percentage of dye removal also depends on the temperature as shown in Fig. 6d. The effect of temperature was studied by varying the temperature from 30 to 70 °C. The %R was found to be highest at 30 °C due to the maximum interactions between adsorbent and dye. With the increase in temperature, the value of percentage removal of dye decreases. As the temperature was increased the electrostatic interactions becomes poor and the bonds started to break which resulted in the reduced adsorption on the surface of adsorbent [58].

Adsorption Kinetics The three different kinetic models were employed to the equilibrium data to understand the adsorption kinetics of MB deeply as the adsorption of dye depends on various physical and chemical interactions

Fig. 5 Mechanism of the removal of MB dye by CG/STPNC ion exchanger



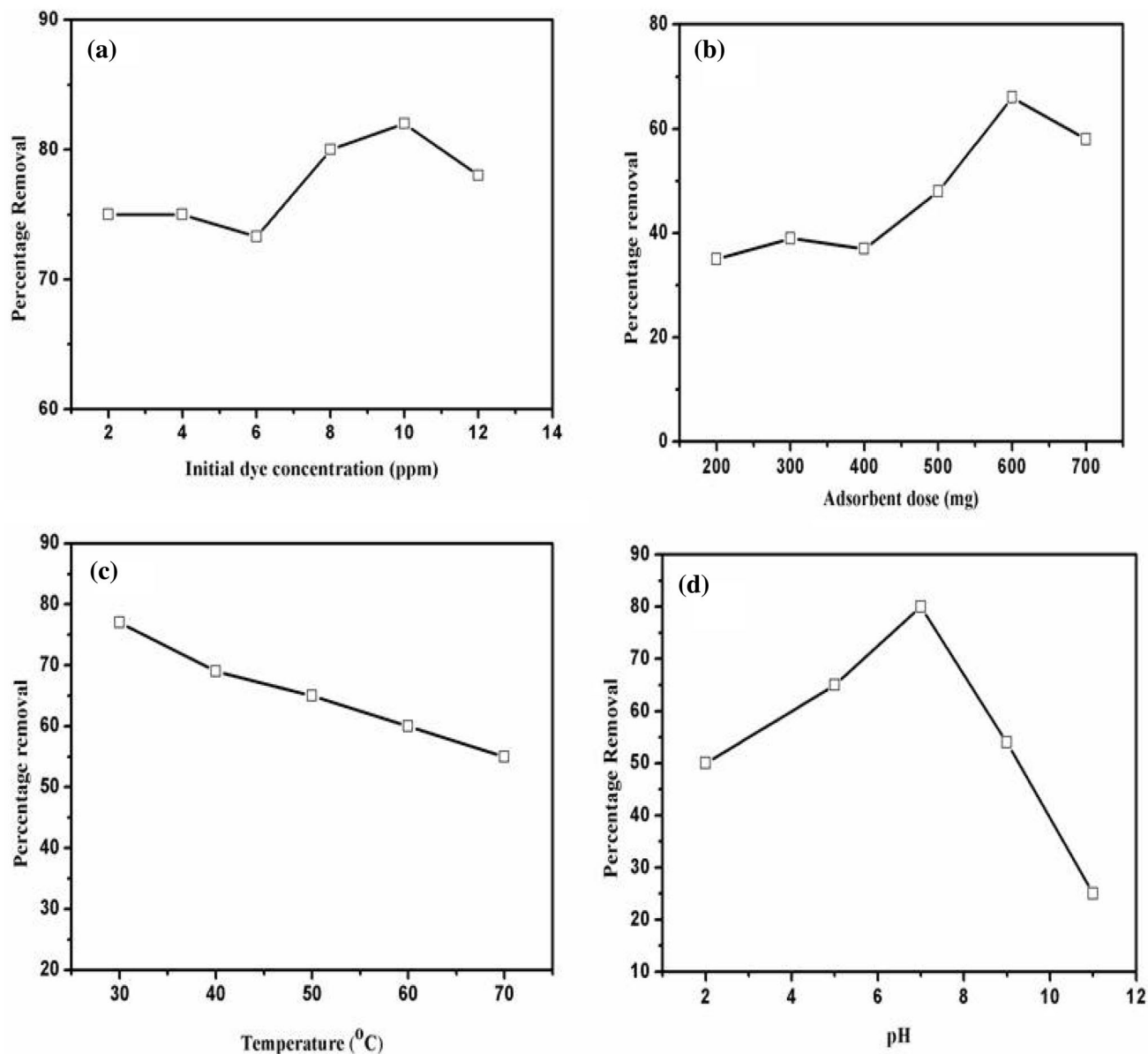


Fig. 6 Optimization of different reaction parameters of removal of MB dye, **a** temperature, **b** initial dye concentration, **c** adsorbent dose, **d** pH

with the adsorbent. The kinetic adsorption of dye was first calculated by Lagergren's Pseudo First order Equation:

$$\ln(q_e - q_t) = \ln q_e - k_1 t \quad (6)$$

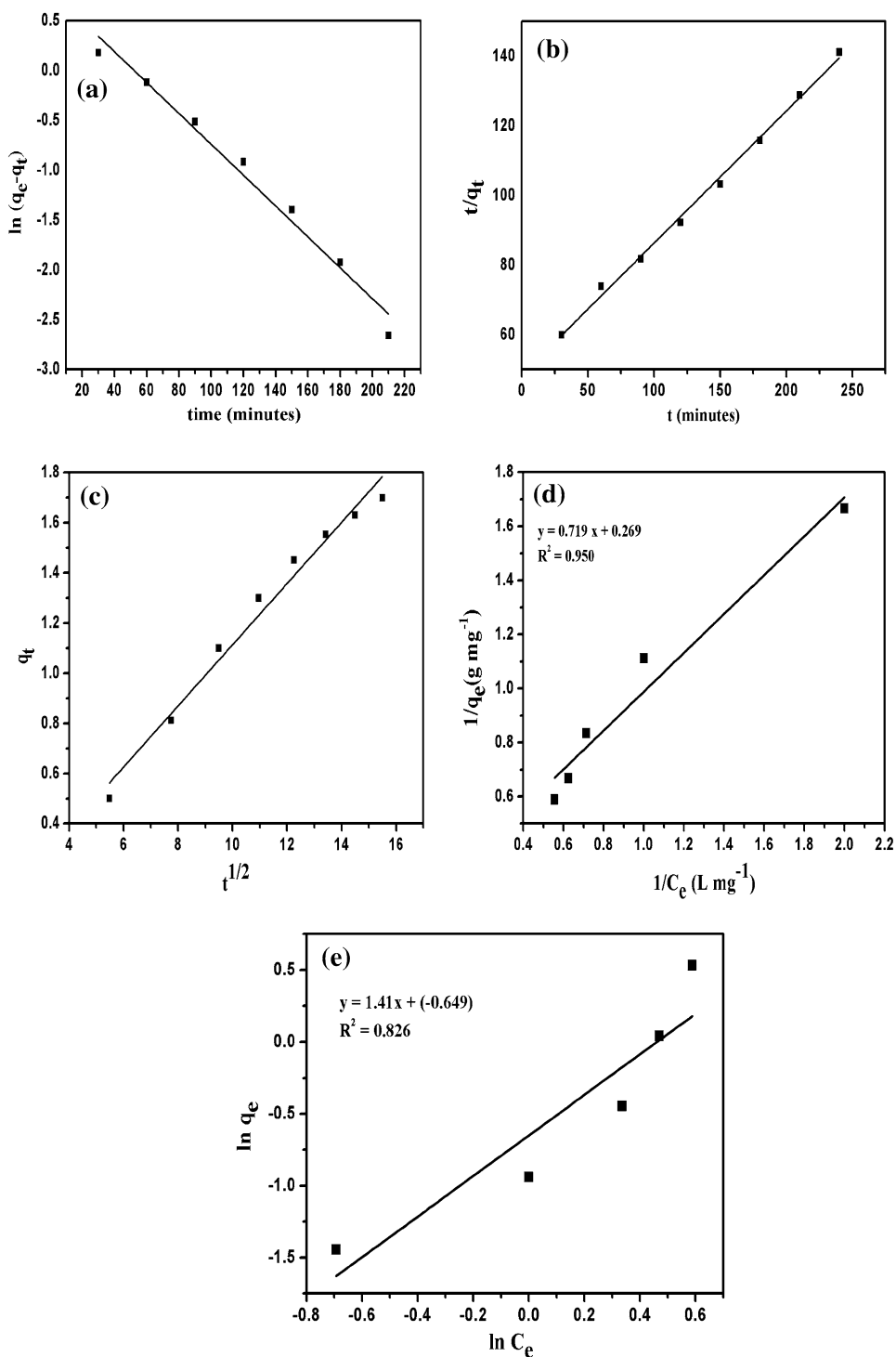
where q_e (mg g^{-1}) and q_t (mg g^{-1}) are the amount of dye adsorbed at equilibrium and time t respectively, k_1 is the first order rate constant. The slope ($-k_1$) and intercept ($\ln q_e$) of the plot (Fig. 7a) between $\ln(q_e - q_t)$ and t were calculated (Table 6). The correlation coefficient value was found to be 0.977 but the value of k_1 was found to be very low (0.015) indicating inability of pseudo-first order to fit into this equilibrium data (Table 7).

The kinetics of dye adsorption was then studied for Ho's and McKay's pseudo-second order by using Eq. (7)

$$\frac{t}{q_t} = \frac{1}{k_2 q_e^2} + \frac{t}{q_e} \quad (7)$$

where q_e and q_t (mg g^{-1}) are the amounts of dye adsorbed at equilibrium and time t and k_2 is the second order rate constant, respectively. The intercept ($1/k_2 q_e^2$) and slope ($1/q_e$) used to calculate the value of k_2 and q_e from the plot (Fig. 7b) between t/q_t versus t . It was confirmed from the values of $q_e = 2.64 \text{ mg g}^{-1}$ and $R^2 = 0.995$ (Table 6) that

Fig. 7 **a** Adsorption kinetics of pseudo-Second order, **b** adsorption kinetics of pseudo-Second order. **c** Adsorption kinetics of intra particle diffusion. **d** Langmuir adsorption isotherm. **e** Freundlich adsorption isotherm



the pseudo-second order kinetic model is applicable for the adsorption of MB dye onto the CG/STPNC ion exchanger over the entire adsorption period. Adsorption of MB dye might be due to chemisorptions. The rate of the slow step depends upon the interactions of MB dye molecules and adsorbent concentration.

The kinetic results were also verified to observe if intra-particle diffusion is the rate determining step for the adsorption of MB on the nanocomposite ion exchanger. So, the kinetic data was also studied by Weber and Morris intraparticle diffusion model (Eq. 8)

$$q_t = k_i t^{0.5} + C \tag{8}$$

Table 6 Kinetic parameters for the adsorption of MB on CG/STPNC

Kinetic model	Kinetic parameter	
Pseudo first order	$k_1 \times 10^{-2}(\text{min}^{-1})$	1.5
	$q_e^{\text{cal}}(\text{mg g}^{-1})$	2.32
	$q_e^{\text{exp}}(\text{mg g}^{-1})$	1.7
	R^2	0.977
Pseudo second order	$k_2 \times 10^{-3}(\text{g mg}^{-1} \text{min}^{-1})$	2.97
	$q_e^{\text{cal}}(\text{mg g}^{-1})$	2.64
	$q_e^{\text{exp}}(\text{mg g}^{-1})$	1.7
	R^2	0.995
Intraparticle diffusion	$k_i \times 10^{-1}(\text{mg g}^{-1} \text{min}^{1/2})$	1.22
	C	-0.10
	R^2	0.977

Table 7 Isotherm parameters for the adsorption of MB on CG/STPNC

Isotherm model	Isotherm constants	
Langmuir	Q_m	3.72
	b	0.37
	R_L	0.21
	R^2	0.950
Freundlich	n	0.71
	k_f	-1.91
	R^2	0.826

where k_i is the intraparticle diffusion rate constant and C is a constant which gives information about boundary layer resistance.

The value of k_i (Table 6) was calculated from the plot of qt versus $t^{0.5}$ (Fig. 7c). The value of the regression coefficient for this model was found to be 0.97 but the plot didn't pass through the origin, which ensured that the intraparticle diffusion is not the only rate determining step. This also confirmed that the adsorption process is a multistep process involving adsorption, diffusion and ion exchange formation [59].

Adsorption Isotherm Langmuir and Freundlich isotherm models were used to determine whether the adsorption of dye was homogeneous or heterogeneous. The Langmuir isotherm for monolayer adsorption is given as:

$$q_e = \frac{Q_m b C_e}{1 + b C_e} \quad (9)$$

where C_e (mg L^{-1}) is the equilibrium concentration of dye, q_e is the amount of dye adsorbed at equilibrium (mg g^{-1}), b is the Langmuir constant and Q_m is monolayer capacity, respectively.

$$\frac{1}{q_e} = \frac{1}{Q_m b C_e} + \frac{1}{Q_m} \quad (10)$$

A plot of $1/q_e$ versus C_e was used to calculate the values of b and Q_m from the intercept and slope, respectively (Fig. 7d).

$$R_L = \frac{1}{1 + b C_o} \quad (11)$$

where C_o is the initial dye concentration (mg L^{-1}). The R_L value depicts whether the isotherm is favourable ($0 < R_L < 1$), unfavourable ($R_L > 1$), linear ($R_L = 1$) or irreversible ($R_L = 0$).

The value of the correlation coefficient (R^2) for the isotherm was found to be 0.95, which is closer to unity so this Langmuir adsorption isotherm is applicable for the adsorption of MB using the CG/STPNC ion exchanger. The shape of Langmuir was determined by the separation factor R_L which is a dimensionless constant (Eq. 11). The value of R_L was found to be 0.21 and again indicated that the Langmuir adsorption isotherm was favourable for the adsorption process in the present study.

The Freundlich isotherm for multilayer adsorption is given by the equation:

$$\ln q_e = \ln k_f + (1/n) \ln C_e \quad (12)$$

where k_f (mg/g) is adsorption capacity, $1/n$ is the heterogeneity factor. The slope ($1/n$) and intercept ($\ln k_f$) were calculated from the plot of $\ln q_e$ and $\ln C_e$ (Fig. 7e). The value of $1/n$ indicates the isotherm to be favorable ($0 < 1/n < 1$), unfavorable ($1/n > 1$) or irreversible ($1/n = 0$).

The $1/n$ value for the adsorption of MB on the CG/STPNC ion exchanger was found to be 1.461, which clearly indicates the adsorption through Freundlich isotherm is unfavourable. The correlation value of 0.826 also supports this. So the correlation value 0.95 suggesting better fit for Langmuir adsorption than Freundlich (0.826). This depicts that the adsorbent surface was homogeneous and process to be a monolayer.

Reusability of the Nanocomposite Ion Exchanger

Stability, efficiency and sustainability of the synthesized CG/STPNC ion exchanger were explored by the percentage dye removal in consecutive adsorption and desorption runs. Regeneration of the nanocomposite ion exchanger was performed by using the 0.03M HCl in five cycles. Dye removal efficiency was not affected much in the first three cycles (Fig. 8). In the fifth cycle, the percentage removal by the nanocomposite ion exchanger was lowered to 52.4% from 82% that clearly revealed the excellent reusability of CG/STPNC ion exchanger. The decrease in the adsorption capacity of the synthesized nanocomposite is attributed to the fact that after every cycle adsorbent gets saturated and results in less availability of the adsorption sites towards removal of methylene blue.

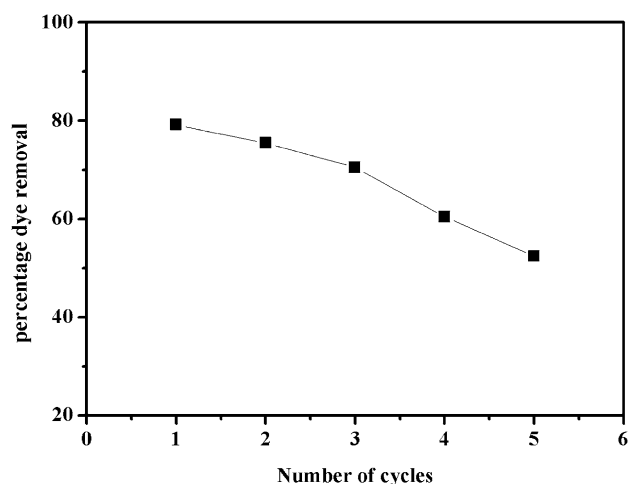


Fig. 8 Reusability analysis of CG/STPNC ion exchanger for MB dye removal

Comparative Studies of the Maximum Monolayer Adsorption Capacity for MB Dye Using Different Adsorbents

A comparative study of the synthesized nanocomposite ion exchanger was performed with other adsorbents reported in the literature [21, 30, 54–58]. It has been done in terms maximum percentage removal of dyes (Table 8). It was found that nanocomposite ion exchanger behaved as adsorbent and ion exchanger simultaneously under coupled

conditions in dye removal investigations. It was noted that CG/STPNC ion exchanger had comparable adsorption capacity with some of the adsorbents listed here. So, CG/STPNC possessed a good potential for the removal of MB dye from an aqueous medium.

Conclusion

The CG/STPNC ion exchanger synthesized by the sol–gel method under vacuum was found to be an efficient device for the removal of MB dye from textile effluents. CG/STPNC ion exchanger was characterised using different characterization techniques such as PXRD, FESEM, HRTEM and FTIR. The ion exchange capacity of the CG/STPNC was found to be 1.8 meq/g. The pH titration studies revealed the bifunctional nature of CG/STPNC. TEM results proved the particle size of the synthesized composite ion exchanger was in nano range and particles size varied from 20 to 90 nm. The distribution studies indicated the higher selectivity of CG/STPNC for Pb (II) and Cu (II). CG/STPNC removes 82% of the methylene blue dye within 4 h. Adsorption kinetic studies confirmed that the pseudo-second order kinetics was found to be applicable with the R^2 value of 0.995 which indicates the chemisorption is the rate determining step. Langmuir adsorption isotherm has shown more compatibility than Freundlich isotherm to the adsorption of MB. Thus, the synthesized CG/STPNC ion exchanger was an efficient device for the removal of toxic dyes like MB from the textile effluents.

Table 8 Comparison of maximum monolayer adsorption capacity for MB dye using different adsorbents

Adsorbent	Dye	Percentage dye removal (%)	References
Pectin @ zirconium (IV) silicophosphate nanocomposite ion exchanger	MB	97.02	[29]
Alginate-Zr (IV) phosphate nanocomposite ion exchanger	MB	97.45	[21]
Pectin–thorium(IV) tungstomolybdate nanocomposite ion exchanger	MB	76	[60]
Brown macroalga	MB	96.99	[61]
anion exchange resin (Zerolit DMF)	MB	98	[62]
CG/STPNC ion exchanger	MB	82	Present work
Chemically modified pine nut shells	MB	98	[63]
MOF nanocomposite	MB	94	[64]

Acknowledgements One of the authors is highly grateful to MHRD for providing financial assistance to carry out research. The author is also thankful to Instrumentation Centre, IIT Roorkee, Materials research centre, MNIT Jaipur, SAIF facility, Punjab University, Chandigarh for different characterization of samples and DST-FIST for providing financial assistance for the procurement of equipment like FTIR and UV–Visible spectrophotometer used in the characterization of the samples.

Compliance with ethical standards

Data availability The raw/processed data required to reproduce these findings cannot be shared at this time as the data also forms part of an ongoing study.

References

- Hui KS, Chao CYH, Kot SC (2005) Removal of mixed heavy metal ions in wastewater by zeolite 4A and residual products from recycled coal fly ash. *J Hazard Mater* 127:89–101. <https://doi.org/10.1016/j.jhazmat.2005.06.027>
- Ayhan S (2008) Adsorption of malachite green onto bentonite: equilibrium and kinetic studies and process design. 115:234–246. <https://doi.org/10.1016/j.micromeso.2008.01.039>
- Sharma J, Chadha AS, Pruthi V et al (2017) Sequestration of dyes from artificially prepared textile effluent using RSM-CCD optimized hybrid backbone based adsorbent-kinetic and equilibrium studies. *J Environ Manag* 190:176–187. <https://doi.org/10.1016/j.jenvman.2016.12.065>
- Shanker U, Rani M, Jassal V (2017) Degradation of hazardous organic dyes in water by nanomaterials. *Environ Chem Lett* 15:623–642. <https://doi.org/10.1007/s10311-017-0650-2>
- Amini M, Ashrafi M (2016) Photocatalytic degradation of some organic dyes under solar light irradiation using TiO₂ and ZnO nanoparticles. *Nano Chem Res* 1:79–86. <https://doi.org/10.7508/ncr.2016.01.010>
- Fu F, Wang Q (2011) Removal of heavy metal ions from wastewaters: a review. *J Environ Manage* 92:407–418. <https://doi.org/10.1016/j.jenvman.2010.11.011>
- Issazadeh H, Engineering G (2015) Preparation of new conductive polymer nanocomposites for cadmium removal from industrial wastewaters Leila Zoleikani, Hossein Issazadeh, Bahman ZareNezhad. 71–80
- Lee SB, Ha DI, Cho SK et al (2003) Temperature/pH-sensitive comb-type graft hydrogels composed of chitosan and poly (*N*-isopropylacrylamide)
- Sharma J, Anand P, Pruthi V et al (2017) RSM-CCD optimized adsorbent for the sequestration of carcinogenic rhodamine-B: kinetics and equilibrium studies. *Mater Chem Phys* 196:270–283. <https://doi.org/10.1016/j.matchemphys.2017.04.042>
- Vermeer AWP, McCulloch JK, Van Riemsdijk WH, Koopal LK (1999) Metal ion adsorption to complexes of humic acid and metal oxides: deviations from the additivity rule. *Environ Sci Technol* 33:3892–3897. <https://doi.org/10.1021/es990260k>
- Zavvar Mousavi H, Seyedi SR (2010) Kinetic and equilibrium studies on the removal of pb (ii) from aqueous solution using nettle ash. *J Chil Chem Soc* 55:307–311. <https://doi.org/10.4067/S0717-97072010000300006>
- Naushad M, AlOthman ZA, Awual MR, Alam MM, Eldesoky GE, Adsorption kinetics, isotherms, and thermodynamic studies for the adsorption of Pb²⁺ and Hg²⁺ metal ions from aqueous medium using Ti(IV) iodovanadate cation exchanger. *Ionics* 2237:224–221. <https://doi.org/10.1007/s11581-015-1401-7>
- Sharma P, Jindal R, Maiti M, Jana AK (2016) Novel organic–inorganic composite material as a cation exchanger from a triterpenoidal system of dammar gum: synthesis, characterization and application. *Iran Polym J*. <https://doi.org/10.1007/s13726-016-0456-2>
- Pathania D, Gupta D, Al-Muhtaseb AH et al (2016) Photocatalytic degradation of highly toxic dyes using chitosan-g-poly(acrylamide)/ZnS in presence of solar irradiation. *J Photochem Photobiol A Chem* 329:61–68. <https://doi.org/10.1016/j.jphotochem.2016.06.019>
- Naushad M, Mittal A, Rathore M, Gupta V (2015) Ion-exchange kinetic studies for Cd(II), Co(II), Cu(II), and Pb(II) metal ions over a composite cation exchanger. *Desalin Water Treat* 54:2883–2890. <https://doi.org/10.1080/19443994.2014.904823>
- Naushad M, AL-Othman ZA, Islam M (2013) Adsorption of cadmium ion using a new composite cation-exchanger polyaniline Sn(IV) silicate: kinetics, thermodynamic and isotherm studies. *Int J Environ Sci Technol* 10:567–578. <https://doi.org/10.1007/s13762-013-0189-0>
- Çay S, Uyanik A, Özaşık A (2004) Single and binary component adsorption of copper(II) and cadmium(II) from aqueous solutions using tea-industry waste. *Sep Purif Technol* 38:273–280. <https://doi.org/10.1016/j.seppur.2003.12.003>
- Naushad M, AL-Othman ZA, Javadian H (2015) Removal of Pb(II) from aqueous solution using ethylene diamine tetra acetic acid-Zr(IV) iodate composite cation exchanger: Kinetics, isotherms and thermodynamic studies. *J Ind Eng Chem* 25:35–41. <https://doi.org/10.1016/j.jiec.2014.10.010>
- Bushra R, Naushad M, Adnan R et al (2015) Polyaniline supported nanocomposite cation exchanger: synthesis, characterization and applications for the efficient removal of Pb²⁺ ion from aqueous medium. *J Ind Eng Chem* 21:1112–1118. <https://doi.org/10.1016/j.jiec.2014.05.022>
- Siddiqi ZM, Pathania D (2003) Studies on titanium(IV) tungstosilicate and titanium(IV) tungstophosphate. II. Separation and estimation of heavy metals from aquatic environments. *Acta Chromatogr* 172–184
- Pathania D, Thakur M, Mishra AK (2017) Alginate–Zr (IV) phosphate nanocomposite ion exchanger: binary separation of heavy metals, photocatalysis and antimicrobial activity. Elsevier, Oxford
- Kullberg L (1984) Edited by A. Clearfield (Texas ASM University). CRC Press, Inc, Raton B, Fl. 1982. 304 pp. \$ 84.50. *Solvent Extr Ion Exch* 2:121–122. <https://doi.org/10.1080/07366298408918440>
- Naushad M (2014) Surfactant assisted nano-composite cation exchanger: Development, characterization and applications for the removal of toxic Pb²⁺ from aqueous medium. *Chem Eng J* 235:100–108. <https://doi.org/10.1016/j.cej.2013.09.013>
- Varshney KG, Khan AA, Siddiqui MS (1989) Synthesis, ion exchange behaviour and characterization of chromium(III) arsenosilicate cation exchanger. *Colloids Surf* 36:405–416. [https://doi.org/10.1016/0166-6622\(89\)80255-0](https://doi.org/10.1016/0166-6622(89)80255-0)
- New AA, Exchanger C, Varshney KG et al (1998) Synthesis and characterization of zirconium. 7353–7358
- Jindal R, Sharma R, Maiti M, Kaur H (2016) In air synthesis of psyllium based organo- inorganic hybrid ion exchanger, its characterization and studies. 1:22–29
- Narayana S, Graduate P (2006) Synthetic inorganic ion exchangers Reetha Nanu Cheruvalath “Studies on some ion exchangers ”
- Saruchi KV, Kaith BS, Jindal R (2016) Synthesis of hybrid ion exchanger for rhodamine B dye removal: equilibrium, kinetic and

- thermodynamic studies. *Ind Eng Chem Res* 55:10492–10499. <https://doi.org/10.1021/acs.iecr.6b01690>
29. Pathania D, Sharma G, Thakur R (2015) Pectin @ zirconium (IV) silicophosphate nanocomposite ion exchanger: photo catalysis, heavy metal separation and antibacterial activity. *Chem Eng J* 267:235–244. <https://doi.org/10.1016/j.cej.2015.01.004>
 30. Pathania D, Gupta D, Agarwal S et al (2016) Fabrication of chitosan-g-poly(acrylamide)/CuS nanocomposite for controlled drug delivery and antibacterial activity. *Mater Sci Eng C* 64:428–435. <https://doi.org/10.1016/j.msec.2016.03.065>
 31. Kaith BS, Sharma J, Kaur T et al (2016) Microwave-assisted green synthesis of hybrid nanocomposite: removal of Malachite green from waste water. *Iran Polym J (English Ed)* 25:787–797. <https://doi.org/10.1007/s13726-016-0467-z>
 32. Rana P, Mohan N, Rajagopal C (2004) Electrochemical removal of chromium from wastewater by using carbon aerogel electrodes. *Water Res* 38:2811–2820. <https://doi.org/10.1016/j.watres.2004.02.029>
 33. Mobasherpour I, Salahi E, Pazouki M (2011) Removal of divalent cadmium cations by means of synthetic nano crystallite hydroxyapatite. *Desalination* 266:142–148. <https://doi.org/10.1016/j.desal.2010.08.016>
 34. Ma Y, Zheng YM, Chen JP (2011) A zirconium based nanoparticle for significantly enhanced adsorption of arsenate: synthesis, characterization and performance. *J Colloid Interface Sci* 354:785–792. <https://doi.org/10.1016/j.jcis.2010.10.041>
 35. Sharma G, Pathania D, Naushad M (2015) Preparation, characterization, and ion exchange behavior of nanocomposite polyaniline zirconium(IV) selenotungstophosphate for the separation of toxic metal ions. *Ionics* 21:1045–1055. <https://doi.org/10.1007/s11581-014-1269-y>
 36. Peng Z, Peng Z, Shen Y (2011) Fabrication and properties of gelatin/chitosan composite hydrogel. *Polym Plast Technol Eng* 50:1160–1164. <https://doi.org/10.1080/03602559.2011.574670>
 37. Mao JS, Zhao LG, Yin YJ, Yao K, De (2003) Structure and properties of bilayer chitosan–gelatin scaffolds. *Biomaterials* 24:1067–1074. [https://doi.org/10.1016/S0142-9612\(02\)00442-8](https://doi.org/10.1016/S0142-9612(02)00442-8)
 38. Albadarin AB, Collins MN, Naushad M et al (2017) Activated lignin–chitosan extruded blends for efficient adsorption of methylene blue. *Chem Eng J* 307:264–272. <https://doi.org/10.1016/j.cej.2016.08.089>
 39. Sharma G, Naushad M, Al-Muhtaseb AH et al (2017) Fabrication and characterization of chitosan-crosslinked-poly(alginate) nanohydrogel for adsorptive removal of Cr(VI) metal ion from aqueous medium. *Int J Biol Macromol* 95:484–493. <https://doi.org/10.1016/j.ijbiomac.2016.11.072>
 40. Kumar A, Guo C, Sharma G et al (2016) Magnetically recoverable ZrO₂/Fe₃O₄/chitosan nanomaterials for enhanced sunlight driven photoreduction of carcinogenic Cr(VI) and dechlorination and mineralization of 4-chlorophenol from simulated waste water. *RSC Adv* 6:13251–13263. <https://doi.org/10.1039/c5ra23372k>
 41. Muhmood T, Xia M, Lei W, Wang F (2018) Under vacuum synthesis of type-I heterojunction between red phosphorus and graphene like carbon nitride with enhanced catalytic, electrochemical and charge separation ability for photodegradation of an acute toxicity category-III compound. *Appl Catal B Environ* 238:568–575. <https://doi.org/10.1016/j.apcatb.2018.07.029>
 42. Therdthai N, Zhou W (2009) Characterization of microwave vacuum drying and hot air drying of mint leaves (*Mentha cordifolia* Opiz ex Fresen). *J Food Eng* 91:482–489. <https://doi.org/10.1016/j.jfoodeng.2008.09.031>
 43. Deng H, Lu J, Li G et al (2011) Adsorption of methylene blue on adsorbent materials produced from cotton stalk. *Chem Eng J* 172:326–334. <https://doi.org/10.1016/j.cej.2011.06.013>
 44. Wang L, Zhang J, Wang A (2008) Removal of methylene blue from aqueous solution using chitosan-g-poly(acrylic acid)/montmorillonite superadsorbent nanocomposite. *Colloids Surf A Physicochem Eng Asp* 322:47–53. <https://doi.org/10.1016/j.colsurfa.2008.02.019>
 45. Mi FL (2005) Synthesis and characterization of a novel chitosan-gelatin bioconjugate with fluorescence emission. *Biomacromol* 6:975–987. <https://doi.org/10.1021/bm049335p>
 46. Sharma G, Kumar A, Pathania D, Sillanpa M (2016) Journal of Industrial and Engineering Chemistry Polyacrylamide @ Zr (IV) vanadophosphate nanocomposite: Ion exchange properties, antibacterial activity, and photocatalytic behavior. *J Ind Eng Chem* 33:201–208. <https://doi.org/10.1016/j.jiec.2015.10.011>
 47. Siddiqi ZM, Pathania D (2003) Titanium(IV) tungstosilicate and titanium(IV) tungstophosphate: two new inorganic ion exchangers. *J Chromatogr A* 987:147–158
 48. Kaith BS, Jindal R, Sharma R (2015) Synthesis of a Gum rosin alcohol-poly(acrylamide) based adsorbent and its application in removal of malachite green dye from waste water. *RSC Adv* 5:43092–43104. <https://doi.org/10.1039/C5RA04256A>
 49. Fain SC, Sorensen L, Vilches OE (2011) Electron diffraction. 1–8
 50. Naushad M, Ahamad T, Al-Maswari BM et al (2017) Nickel ferrite bearing nitrogen-doped mesoporous carbon as efficient adsorbent for the removal of highly toxic metal ion from aqueous medium. *Chem Eng J* 330:1351–1360. <https://doi.org/10.1016/j.cej.2017.08.079>
 51. Alqadami AA, Naushad M, Allothman ZA, Ghfar AA (2017) Novel metal-organic framework (MOF) based composite material for the sequestration of U(VI) and Th(IV) metal ions from aqueous environment. *ACS Appl Mater Interfaces* 9:36026–36037. <https://doi.org/10.1021/acsami.7b10768>
 52. Ovchinnikov O, Chernykh S, Smirnov MS et al (2007) Analysis of interaction between the organic dye methylene blue and the surface of AgCl (I) microcrystals. *J Appl Spectrosc* 74:731–737
 53. Vargas AMM, Cazetta AL, Kunita MH et al (2011) Adsorption of methylene blue on activated carbon produced from flamboyant pods (*Delonix regia*): Study of adsorption isotherms and kinetic models. *Chem Eng J* 168:722–730. <https://doi.org/10.1016/j.cej.2011.01.067>
 54. Su F, Lu C, Hu S (2010) Adsorption of benzene, toluene, ethylbenzene and p-xylene by NaOCl-oxidized carbon nanotubes. *Colloids Surf A Physicochem Eng Asp* 353:83–91. <https://doi.org/10.1016/j.colsurfa.2009.10.025>
 55. Fu Y, Huang Y, Hu J (2018) Preparation of chitosan/MCM-41-PAA nanocomposites and the adsorption behaviour of Hg (II) ions. *R Soc Chem* 171927
 56. Kaur S, Jindal R, Kaur Bhatia J (2018) Synthesis and RSM-CCD optimization of microwave-induced green interpenetrating network hydrogel adsorbent based on gum copal for selective removal of malachite green from waste water. *Polym Eng Sci* 1–11. <https://doi.org/10.1002/pen.24851>
 57. Das S, Subuddhi U (2013) Cyclodextrin mediated controlled release of naproxen from pH-sensitive chitosan/poly(vinyl alcohol) hydrogels for colon targeted delivery. *Ind Eng Chem Res* 52:14192–14200. <https://doi.org/10.1021/ie402121f>
 58. Jindal R, Sharma R, Maiti M, Sharma A (2017) Synthesis and characterization of novel reduced gum rosin–acrylamide copolymer based bimetallic nanogel and their investigation for antimicrobial activity. *Polym Bull* 74:24–30
 59. Ho YS, McKay G (1998) Sorption of dye from aqueous solution by peat. *Chem Eng J* 70:115–124. [https://doi.org/10.1016/S1385-8947\(98\)00076-X](https://doi.org/10.1016/S1385-8947(98)00076-X)
 60. Gupta VK, Agarwal S, Pathania D et al (2013) Use of pectin-thorium (IV) tungstomolybdate nanocomposite for photocatalytic degradation of methylene blue. *Carbohydr Polym* 96:277–283. <https://doi.org/10.1016/j.carbpol.2013.03.073>
 61. Daneshvar E, Vazirzadeh A, Niazi A et al (2017) Desorption of Methylene blue dye from brown macroalgae: effects of operating

- parameters, isotherm study and kinetic modeling. *J Clean Prod* 152:443–453. <https://doi.org/10.1016/j.jclepro.2017.03.119>
62. Khan MA, ALOthman ZA, Naushad M et al (2015) Adsorption of methylene blue on strongly basic anion exchange resin (Zerolit DMF): kinetic, isotherm, and thermodynamic studies. *Desalin Water Treat* 53:515–523. <https://doi.org/10.1080/19443994.2013.838527>
63. Naushad M, Ali Khan M, Abdullah Alothman Z et al (2016) Adsorption of methylene blue on chemically modified pine nut shells in single and binary systems: isotherms, kinetics, and thermodynamic studies. *Desalin Water Treat* 57:15848–15861. <https://doi.org/10.1080/19443994.2015.1074121>
64. Alqadami AA, Naushad M, Alothman ZA, Ahamad T (2018) Adsorptive performance of MOF nanocomposite for methylene blue and malachite green dyes: kinetics, isotherm and mechanism. *J Environ Manag* 223:29–36. <https://doi.org/10.1016/j.jenvman.2018.05.090>